

Secret-Free Device Pairing in the mmWave Band

Ziqi Xu[†] Jingcheng Li[†] Yanjun Pan[‡] Ming Li[†] Loukas Lazos[†]

[†] Department of Electrical and Computer Engineering, University of Arizona

[‡] Department of Computer Science and Computer Engineering, University of Arkansas

Email: [†] {z xu1969, jli2972, lim, llazos}@arizona.edu, [‡] yanjunp@uark.edu

ABSTRACT

Many Next Generation (NextG) applications feature devices that are capable of communicating and sensing in the Millimeter-Wave (mmWave) bands. Trust establishment is an important first step to bootstrap secure mmWave communication links, which is challenging due to the lack of prior secrets and the fact that traditional cryptographic authentication methods cannot bind digital trust with physical properties. Previously, context-based device pairing approaches were proposed to extract shared secrets from common context, using various sensing modalities. However, they suffer from various limitations in practicality and security.

In this work, we propose the first secret-free device pairing scheme in the mmWave band that explores the unique physical-layer properties of mmWave communications. Our basic idea is to let Alice and Bob derive common randomness by sampling physical activity in the surrounding environment that disturbs their wireless channel. They construct reliable fingerprints of the activity by extracting event timing information from the channel state. We further propose an uncoordinated path hopping mechanism to resolve the challenges of beam alignment for activity sensing without prior trust. A key novelty of our protocol is that it remains secure against both co-located passive adversaries and active Man-in-the-Middle attacks, which is not possible with existing context-based pairing approaches. We implement our protocol in a 28GHz mmWave testbed, and experimentally evaluate its security in realistic indoor environments. Results show that our protocol can effectively thwart several different types of adversaries.

1 INTRODUCTION

The increasing demand for higher data rates has pushed wireless technologies to millimeter wave (mmWave) bands where bandwidth is abundant. The physics of signal propagation at such short wavelengths offer some security advantages compared to typical microwave communications due to the substantial signal attenuation (which is proportional to the center frequency) and susceptibility to blockage [30]. For instance, eavesdropping becomes more challenging as mmWave transmissions are highly-directional and do not travel through physical barriers. Nevertheless, common security threats such as eavesdropping, message injection, message modification, impersonation, and Man-in-the-Middle (MitM) attacks are still feasible [5, 38] if wireless transmissions are left unprotected.

The widely adopted approach for protecting wireless links is to incorporate cryptographic solutions relying on asymmetric and symmetric cryptosystems [35]. However, such solutions require extensive key management for establishing and maintaining trust, which can pose scalability challenges. Moreover, digital keys created from pseudo-random generators do not bind the devices that use them with any surrounding physical property. For instance,

two devices that use a symmetric key to encrypt communications over a public channel, cannot verify any other physical property such as location. Extending trust to the physical world has become prevalent with the advent of Next Generation (NextG) communications, where many applications seamlessly integrate the cyber and physical worlds (e.g., industrial automation, connected healthcare, connected autonomous vehicles).

A complementary approach to pre-loading pseudo-randomly generated secrets is to generate secrets from common sources of randomness that exhibit high spatial and temporal dynamics [52]. The main idea is that two co-located devices can independently sample a high-entropy physical property to derive a common key. The high spatial correlation of the samples at the locations of the legitimate devices compared to the low correlation at the adversary's location offers the security advantage in the key generation process. The so-called context-based key generation methods have notable advantages such as reduced user efforts, perpetual key renewal, and high level of security to remote adversaries. Commonly explored physical modalities include light [25], sound [25, 32, 51], wireless channel reciprocity [19, 24], ambient RF signals [11, 23], human operation [17, 56], as well as multi-modal approaches [8, 10].

1.1 Motivation and Challenges

Context-based secure pairing methods present numerous challenges. First, many modalities (e.g., light, sound) suffer from low entropy, requiring long sampling times to agree on common bits. They also require all devices to possess a common sensing capability, which may not be available in IoT applications. More importantly, they require physical access control to guarantee security. The threat model assumes that the adversary has no physical access to the environment where measurements take place. Moreover, they are susceptible to active attacks where an adversary alters the physical environment to make key generation predictable. RF modalities exhibit high entropy in rich-multipath environments, which are common in sub-6 GHz communications where the majority of prior works have been operating [19, 22, 23]. However, mmWave communications follow geometric channel models [3] with very few reflections contributing to the channel uncertainty. Moreover, RF based methods have been shown to be vulnerable to active attacks where an adversary, Mallory, opportunistically injects signals to make bit extraction predictable [7].

To counter the limitations of prior works and to transition device pairing protocols to NextG networks, we explore the unique PHY-layer properties of mmWave communications to develop a novel secret-free device pairing protocol. Specifically, Alice and Bob independently derive common randomness by sampling physical activity that disturbs their wireless channel in the presence of Mallory. Wireless paths are interrupted by artificial or naturally-occurring motion (e.g., human motion) within the environment at random

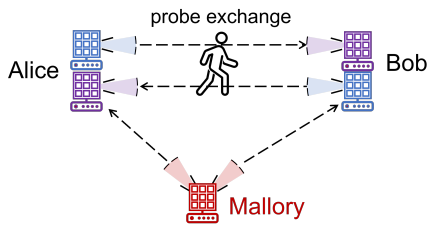


Figure 1: Alice and Bob use mmWave probes to detect physical activity in the line-of-sight path and agree on a common key. Mallory cannot sample the same activity.

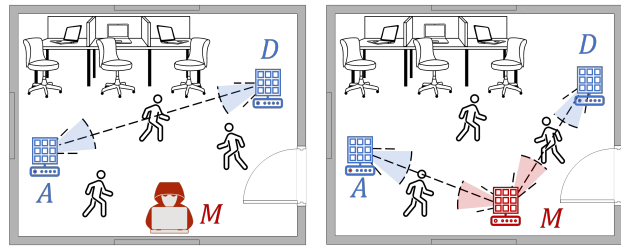
times. This interruption is sensed by measuring the amplitude of channel state information (CSI) over the distinct paths that connect Alice and Bob. An example is shown in Figure 1. The antennas of Alice and Bob are aligned over the line-of-sight (LOS) path. The LoS path is interrupted by physical activity. Even if Mallory is in the same environment, she observes a different path and therefore cannot measure the same CSI variations. Mallory could observe the physical activity using other modalities such as vision; however, it is exceedingly difficult to estimate the impact of motion on the wireless channel at a very fine time scale, thus leaving the pairing process secure.

There are several key technical challenges to design such a protocol that senses ambient activity for device pairing in the mmWave band. First, due to the small wavelength of mmWave signals, the CSI (and its amplitude) in the mmWave band is very sensitive to small disturbances to the channel, and channel reciprocity may not hold. Directly adopting measured CSI samples for key agreement will introduce a high bit mismatch rate. Second, since mmWave communication is highly directional, devices must have their beams aligned on the direction(s) where activity exists to be able to sense it. However, neither prior knowledge nor prior trust is available to support such beam alignment in a secure manner. Third, the protocol must be resistant against a wide range of threats, not only co-present passive adversaries but also active attacks such as Man-in-the-Middle. This should be achieved without prior trust.

1.2 Main Contributions

In this paper, we propose a novel context-based key pairing protocol for devices that operate in the mmWave band, with merely in-band RF communication. The basic protocol is called JellyBean, which exploits the pencil-like beams used in mmWave communications to detect disturbances (channel blockage) to the wireless channel due to physical motion from natural or artificial activity. To solve the first challenge, we extract the timing of activities from the CSI magnitude to generate a fingerprint of the ambient environment, which is used as a common source of randomness between Alice and Bob. A passive adversary is unable to infer the secret if observing the same activities from a different vantage point due to the high directionality of mmWave transmissions.

Our basic pairing protocol is still vulnerable to a passive adversary that is located in close proximity to either Alice or Bob and aligned in the sampled path or an active adversary that launches beam-stealing attacks [38]. Thus, we further introduce Jellybean+



(a) Passive attack (b) Active beam-stealing attack

Figure 2: Threat model (a) Mallory passively observes the same environment as A and D, (b) Mallory launches an active beam stealing attack.

which incorporates an uncoordinated path-hopping (UPH) mechanism. UPH takes advantage of the electronic antenna steering capabilities at mmWave to randomize the paths sampled by Alice and Bob in a similar way as channel-hopping randomizes the communication frequency. Without knowledge of which paths are sampled at any point in time, a co-located adversary cannot construct fingerprints similar to Alice and Bob. A notable difference from frequency hopping is that in UPH no common hopping sequence is necessary for activity sensing.

We experimentally evaluate the performance and security of our protocols on a 28GHz mmWave testbed in typical indoor environments. Our experiments demonstrate that the bit mismatch rate between Mallory and Alice or Bob far exceeds that of the legitimate devices, allowing for secure pairing in reasonable time. We also show that the key derived from physical activities satisfies the NIST randomness tests [6]. To further demonstrate the security of our protocols, we analyze both passive attacks involving eavesdropping as well as recording of physical activities using cameras.

The key novelty of Jellybean compared to the state-of-the-art context-based pairing protocols is that it remains secure even if Mallory (a) Mallory is co-located in the same environment and can observe the ongoing physical activity and (b) launches an active attack. In fact, Jellybean+ remains secure even if Mallory is at the same location as Alice or Bob.

2 SYSTEM AND THREAT MODEL

2.1 System Model

The system consists of an access point A and a legitimate device D located in a typical indoor environment. Both devices operate in the mmWave band and are equipped with electronically-steerable directional antennas. Their antennas can be aligned using the Sector Level Sweep (SLS) protocol of IEEE 802.11ad [2], although any suitable beam alignment protocol can be used. The devices aim at securely pairing and establish a common secret $k_A = k_D = k$. The devices do not share any prior secrets.

2.2 Threat Model

The goal of the adversary is to learn the common secret k derived by A and D during the pairing process. The adversary is equipped with an electronically steerable antenna that can be pointed to any direction. Most prior context-based pairing methods assume physical access control [8, 10, 25, 32]. The adversary is assumed

to be unable to observe the environment sampled by A and D . For instance, the legitimate devices and the adversary are separated by a physical barrier such as a wall that makes physical properties such as light, sound, and human activity unobservable. Our threat model breaks this rather artificial assumption and allows the adversary to be in the same environment as A and D , as shown in Figure 2(a).

The adversary has full knowledge of the context-based pairing protocol executed by the legitimate devices. However, she does not control the physical activities taking place in the environment as this is easily visually detected. Mallory could be either passively trying to derive the secret k or launch an active attack.

Passive attacks: A passive Mallory can steer her antenna to A and D respectively, to eavesdrop on any messages exchanged between the two parties. Moreover, Mallory can steer her antenna to any other desired direction including the location where physical activities may take place. Mallory can position herself at a location of her own choosing. This assumption is fairly strong, as the presence of Mallory in private spaces can be easily detected. However, it may hold for public spaces. Moreover, it provides the worst-case analysis on the protocol security. Finally, Mallory may have access to a separate modality such as vision (camera) that allows her to observe the physical activities occurring in the environment. The resolution is limited by the modality used (e.g., frame rate).

Active Attacks. Mallory can inject her own signals to compromise the device pairing process. We assume that the purpose of signal injection is the compromise of the secret derived between A and D [26] and not a denial-of-service (DoS) attack. The latter is fairly easy to launch against device pairing protocols using interference attacks such as selective-jamming. Moreover, Mallory can launch a beam-stealing attack that allows the implementation of a MitM adversary in directional mmWave communications [38]. The main idea of a beam stealing is shown in Figure 2(b). Mallory manipulates the beam alignment process between A and D by forging sector sweep frames with high RSS. A and D can only communicate through Mallory as their antennas are aligned to M . Mallory can then launch a MitM attack against the pairing process between A and D . We note that although several methods have been proposed to add authentication to the beam alignment process [4, 36, 44, 45], they require prior trust to be established, or training for the purpose of fingerprinting and thus are not applicable in the absence of trust.

3 PROTOCOL DESIGN

We design a context-based secure pairing protocol suitable for mmWave communications. Security is drawn from the random physical motions in the environment (e.g., human activity). The motions could occur naturally in high-traffic scenarios, or could be artificially induced by the user. We emphasize that although physical activity has been used as a source of randomness in prior works [17, 56], it affects mmWave transmissions in a different way than microwave transmissions. In microwave frequencies, motion is observed primarily via multipath and scattering whereas in mmWave, it is primarily observed as blockage, which is path-specific. This path specificity provides an opportunity to build stronger security compared to microwave-based methods, that are not to be vulnerable to non-LoS sensing [58].

The legitimate devices A and D align their antennas over a feasible communication path using a beam alignment protocol such as the sector level sweep process in 802.11ad [2]. The random motions in the environment disrupt the $A - D$ channel in an unpredictable manner in terms of timing and duration. These disruptions are unique to the path between $A - D$ due to the high antenna directionality of mmWave communications and prevent Mallory from recording similar channel disruptions by observing the same physical activity from a different vantage point.

Some vantage points may allow the observation of similar disruptions as the $A - D$ channel. For instance, when M is aligned with the $A - D$ LoS channel. To secure against these special locations, we add diversity in the paths sampled for activity. Rather than relying on a single path, A and D randomly hop to other available paths (e.g., through a reflection) in an uncoordinated fashion, thus randomizing the direction over which activity is observed. Even if the adversary can measure channel activity on all paths (e.g., by fast switching or deploying multiple antennas), she does not know the antenna directions for A and D , thus being unable to infer which activity is used in key generation. Our uncoordinated path hopping method resembles frequency hopping to avoid eavesdropping and jamming [39], but it occurs without a commonly shared hopping sequence and in the space domain.

3.1 Fingerprinting Physical Activity

The core security primitively used in our secure key extraction process is the unpredictability of how physical activity impacts a mmWave path at a fine time scale. To fingerprint physical activity, the two legitimate devices A and D align their antennas over a feasible communication path (e.g., the LoS path), as shown in Figure 2(a). The two devices exchange probe messages to measure the CSI amplitude independently. These measurements are processed to extract the start and end time of the physical activity, which is used to independently derive common bits. We emphasize, that contrary to previous CSI-based methods that exploit channel reciprocity [24], we do not use the CSI amplitude directly for key extraction. This is because the CSI has low entropy in mmWave frequencies due to its geometric nature when the path is not disrupted and channel reciprocity breaks under motion on the sensed path.

The main challenge lies in independently processing the CSI samples to achieve a high bit agreement rate while maintaining the entropy provided by the physical motion. We meet this challenge by applying the processing steps shown in Figure 3. First, the CSI samples are denoised and smoothed to filter inherent channel fluctuations introduced by the fine nature of CSI measurement in mmWave. Then, we apply threshold detection to convert CSI sample sequences to a bitstream indicating the presence or absence of activity. Finally, we encode the bitstream to increase the entropy of the derived common secret. We describe each step in detail for device A . The same process is applied at D .

1. Channel sounding. To sense physical activity, devices A and D exchange probes used for channel sounding [29]. The exchange of two probes completes one probing round. At the end of N rounds, the CSI samples are organized into sets CSI_A and CSI_D , respectively. We focus on set CSI_A and drop the A subscript for ease of notation. The CSI set is denoted by $CSI = \{c_1, c_2, \dots, c_K\}$ and each c_i is the

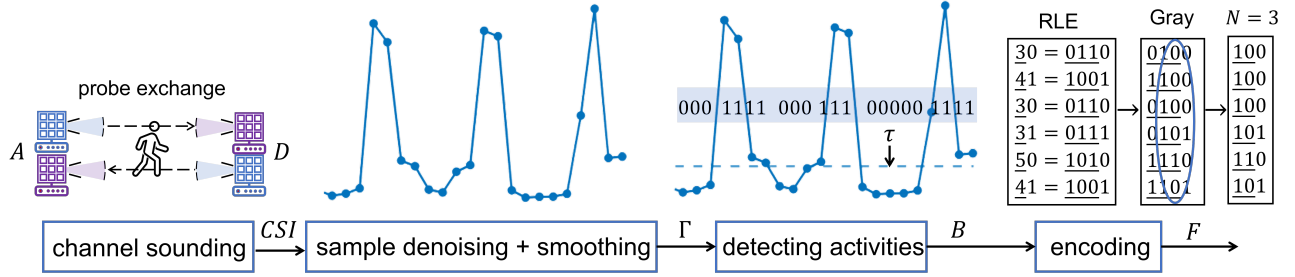


Figure 3: Workflow of the activity fingerprinting process.

set of samples collected per subcarrier. The probes are relatively short, containing a preamble and the unauthenticated device ID.

2. Sample denoising and smoothing. To reduce the noise in CSI measurements, the wavelet transform is applied on each c_i [54]. As channels may be affected differently at various subcarrier frequencies, we compute the cross-correlation between the CSI amplitude samples at each subcarrier and the center subcarrier $K/2$. For two subcarriers i and j with CSI sample sequences c_i and c_j the cross-correlation is given by

$$\rho(i, j) = \frac{1}{\alpha N - 1} \sum_{k=1}^{\alpha N} \left(\frac{c_i(k) - \mu_{c_i}}{\sigma_{c_i}} \right) \left(\frac{c_j(k) - \mu_{c_j}}{\sigma_{c_j}} \right) \quad (1)$$

where μ_{c_i} and σ_{c_i} are the mean and variance of set c_i and α is the number of CSI samples extracted per probe and per subcarrier. The sample sets c_1, c_2, \dots, c_K are ranked according to their cross-correlation with the $K/2^{th}$ subcarrier and only the top half is retained. The new set of samples is denoted by $CSI = \{c_1, c_2, \dots, c_{K/2}\}$ where the set indices correspond to the ranked list of subcarriers.

To further alleviate the high sensitivity of the CSI amplitude measurements in the mmWave channel, we apply a W_m -point moving variance operation to the CSI amplitude along each subcarrier set c_i . Given a set of samples $c_i = \{c_i(1), c_i(2), \dots, c_i(\alpha N)\}$, a W_m -point moving variance for a sample $c_i(j)$ is computed by

$$MV(c_i(j)) = \frac{1}{W_m - 1} \sum_{c(m) \in X_j} (c(m) - \mu_j)^2,$$

where $X_j = \{c_i(j - \lfloor \frac{W_m-1}{2} \rfloor), \dots, c_i(j), \dots, c_i(j + \lfloor \frac{W_m-1}{2} \rfloor)\}$ and μ_j denotes the mean of X_j . We opt to use CSI amplitude variance to capture changes in the CSI amplitude because they are indicative of channel blockage. The moving variance operator is applied to smooth the rapid fluctuations. In the next step, the W_m -point moving variance is averaged over the $K/2$ highest correlated subcarriers to produce a single time series of CSI amplitude, denoted as $\mathcal{T} = \{c(1), c(2), \dots, c(\alpha N)\}$. Finally, to cope with the lack of perfect channel reciprocity and the sensitivity of the mmWave channel to small geometry changes [57], an averaging window of W_s is applied across \mathcal{T} to downsample it by a factor of W_s . The final CSI sequence is denoted by Γ and has a size of $\lfloor \alpha N / W_s \rfloor$ samples.

3. Detecting Activity. Physical activity on a time series Γ is inferred by using threshold-based detection [31]. The process generates a bit sequence B by comparing every sample in Γ with a

detection threshold τ :

$$b(i) = \begin{cases} 1, & \gamma(i) \geq \tau, \\ 0, & \text{otherwise.} \end{cases}$$

The threshold τ is defined as the average over the ℓ lowest CSI amplitude samples in Γ , where ℓ corresponds to a short time duration (e.g., one second). Given the time scale of physical motion, this duration will correspond to a period of inactivity.

4. Encoding. Due to the high sampling rate relative to the speed of any physical motion, bit sequence B consists of many consecutive zero bits (inactivity) followed by consecutive one bits (activity), thus having relatively low entropy. The random part of the physical motion sensed by the probes lies in the start time and duration of the channel disruption. To encode that information alone, we apply run-length encoding (RLE) to transform sequence B into blocks. In RLE, each block of consecutive bits (zeros or ones) is encoded to a counter representing the block length (duration), followed by the block's bit value (activity or inactivity). An example of the application of RLE to an example B is given below (the underlined bits represent the block counter).

$$\begin{aligned} B &= 000000 & 1111 & 000 & 111 & 00000 & 1111 \\ RLE[B] &= \underline{60} & \underline{41} & \underline{30} & \underline{31} & \underline{50} & \underline{41} \\ &= \underline{1100} & \underline{1001} & \underline{0110} & \underline{0111} & \underline{1010} & \underline{1001} \end{aligned}$$

Additionally, we apply Gray encoding to reduce the mismatch between the sequences generated by A and D due to slight mismatches in the block lengths. The number of bits used in Gray code is determined by the longest consecutive bits counted by RLE. In the example, the longest consecutive bit is 6. So we use a 3-bit Gray code in each block. In Gray encoding, two successive counters differ by exactly one bit. The Gray-encoded sequence for the example above is represented by S :

$$S = \underline{1010} \quad \underline{1101} \quad \underline{0100} \quad \underline{0101} \quad \underline{1110} \quad \underline{1101}$$

The final step is to truncate each block to the same length, so that events contribute equally to the final sequence. We achieve this by retaining N least significant bits (LSBs) from each gray-coded block. We retain LSBs because they are harder to predict and thus increase the entropy of the sequence. The final sequence upon the application of truncation of $N = 3$ in the running example is

$$F = 010\ 101\ 100\ 101\ 110\ 101.$$

Sequence F corresponds to the final bit sequence that will be used as an activity fingerprint in the agreement to a common key. At the

end of the independent CSI measurement processing, each device A and D has computed F_A and F_D , respectively.

3.2 The Jellybean Pairing Protocol

We integrate the activity fingerprinting process into a secure device pairing protocol called *Jellybean*. The Jellybean protocol allows A and D establish a common secret k and prevents Mallory from learning k . Moreover, it provides authentication through presence. If M were to execute the same protocol with A (either asynchronously or in parallel), she would establish a different secret. The protocol consists of the activity fingerprinting (AF) phase followed by the key agreement phase, which is a standard fuzzy-commitment based key agreement [15]. The two phases are illustrated in Figure 4 and described below.

Initialization

- (1) A and D align their antennas using a beam alignment protocol [2].
- (2) A and D agree on parameters W_m, W_s, N , and the Reed-Solomon code RS . The parameters could also be preset.

Activity Fingerprinting (AF)

- (5) D and A execute probing rounds and collect CSI_D and CSI_A , respectively.
- (6) D and A generate fingerprints F_D and F_A , respectively, using the activity fingerprinting process described in Section 3.1.

Key Agreement

- (7) A generates a random secret key k and creates commitment $\delta_A = F_A \ominus ENC_{RS}(k)$, where \ominus denotes subtraction in a Galois Field of \mathbb{F}_q , and $ENC_{RS}(\cdot)$ is an RS encoder. A appends $h(k)$ to δ_A and sends the resulting value to D , where $h(\cdot)$ is a secure hash function.
- (8) Upon receiving the commitment δ_A and $h(k)$, D opens the commitment by decoding secret $k' = DEC_{RS}(F_D \ominus \delta_A)$ using its independently derived fingerprint F_D , where $DEC_{RS}(\cdot)$ is the RS decoding function. D then verifies $h(k') \stackrel{?}{=} h(k)$. If the verification succeeds, D accepts the secret. Otherwise, it aborts the pairing process.

The key agreement phase is an application of a fuzzy commitment scheme [15] that has been widely used in context pairing [8, 10, 25]. It can reconcile two similar sequences that differ up to the error correction capability of the selected error correcting code. To conceal the secret k , A computes $\delta_A = F_A \ominus ENC_{RS}(k)$ which reveals no information about k (k is pseudo-random and F_A is unknown to M). Upon receiving the commitment δ_A , D can open the commitment by applying $k' = DEC_{RS}(F_D \ominus \delta_A)$ and recover k' . The value k' is equal to k only if the Hamming distance between F_D and F_A is below the error-correcting capability of the RS code. Finally, the integrity of k' is checked using the attached hash $h(k)$.

4 PARAMETER SELECTION AND SECURITY EVALUATION

In this section, we show how to select the parameters of Jellybean to achieve correctness (secure pairing of a legitimate device) and soundness (leakage of k to Mallory). We further experimentally evaluate Jellybean in terms of performance and security.

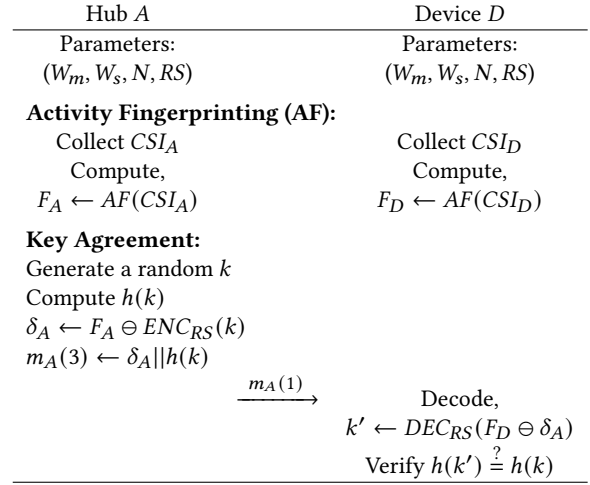


Figure 4: The Jellybean pairing protocol.

4.1 Evaluation Metrics

To evaluate the security and performance of Jellybean, we employ the following metrics that are commonly used for context-based pairing methods.

Bit Mismatch Rate (BMR): the ratio of the Hamming distance between two fingerprints over the fingerprint length. The BMR between F_A and F_D is used as a metric for protocol correctness, whereas the BMR between F_A and F_M is used as a metric for protocol soundness.

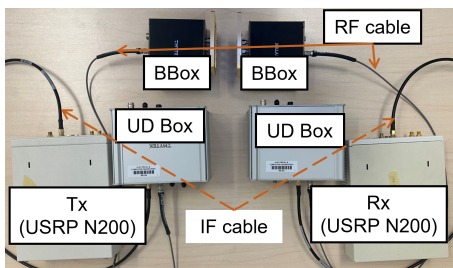
Secret Bit Rate (SBR): the average number of bits extracted per any activity interrupting the A - D channel. Here, we define the SBR per activity as opposed to per unit of time, because the activity rate could vary depending on the environment.

Approximate Entropy (ApEn): A measure of the randomness and unpredictability of a time series. It is preferred over entropy because it provides a more accurate measure of randomness for finite-length series [27].

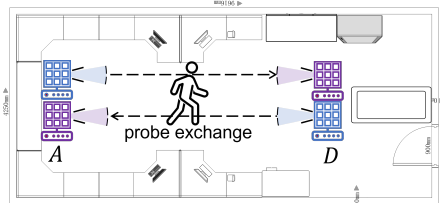
The Jellybean protocol parameters involve tradeoffs between security and performance. For example, the RS code needs to be carefully selected to allow legitimate devices to pair but prevent Mallory from inferring the common key. We study these tradeoffs by co-evaluating correctness and soundness.

4.2 Experiment Setup

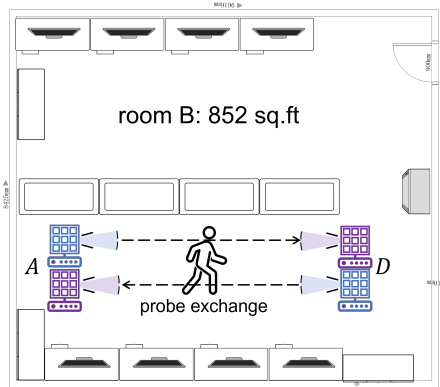
Our experimental setup consisted of USRPs and connected to the TMYTEK mmWave platform [1]. Specifically, we implemented the baseband functionality of A , D and M on USRP N200s. Each USRP was connected to a TMYTEK up-down (UD) converter that upsampled the signal from the sub-6GHz band to a center frequency of 28GHz with 160MHz bandwidth. Transmission took place via a directional BBox lite patch antenna with 16 elements. The antenna supports electronically steerable sectors with half-power beamwidth of 30° , covering the plane with 12 non-overlapping sectors. The maximum transmit power of the USRPs was 30dBm. On the receiver side, the captured 28 GHz signal was down-converted and processed by the USRP. The platform configuration is shown in Figure 5(a).



(a) device connection of each link



(b) Room A, 438 sq.ft



(c) Room B, 852 sq.ft

Figure 5: Experiment setup and topologies.

The exchanged probes consisted of 1,460 bytes and were transmitted using a 5MHz bandwidth over 52 subcarriers. The sampling rate for the USRPs was set to 5 MHz enabling the collection of 3,100 CSI samples for each subcarrier per second. The probing process for CSI measurements requires rapid and continuous switching between signal transmission and reception. Due to the half-duplex capabilities of USRPs N200 and their slow switching capabilities, we performed the probing between A and D using two horizontally-aligned links, as shown in Figures 5(b) and 5(c), where each mmWave communication link consists of the setting in Figure 5(a). Figures 5(b) and 5(c) also show the layout of the two office rooms where we conducted our experiments.

We studied both artificial and natural motions within the environment. To create artificial motions in the A - D channel, we waived a hand vertically across one of the antennas to disrupt the channel. The hand was waived at natural speeds and also horizontally to disrupt any paths beyond the LoS. The artificial motion reflects a scenario where a user is instructed to waive his hand across the device that he intends to pair and provides a usable and quick way for device pairing.

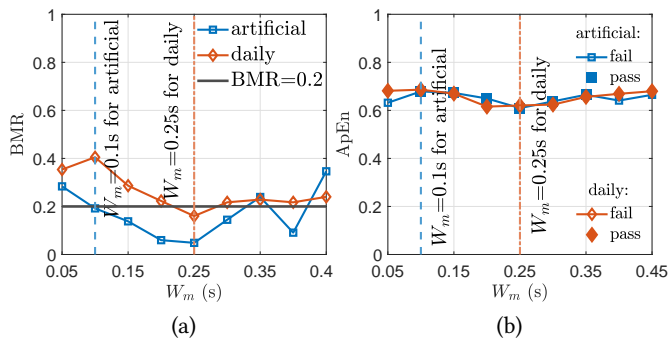


Figure 6: (a) BMR as a function of W_m and (b) ApEn as a function of W_m .

For natural motions, the office occupants walking through the space disrupting different paths at different times. The natural motion reflects a scenario where the natural movement in the space is exploited to pair device as well as continuously renew trust.

4.3 Parameter Selection

The Jellybean protocol is controlled by three parameters: the moving variance window W_m , the averaging window W_s , the number of retained LSBs N in each RLE block, and the RS code for key agreement. In this section, we show how to select these parameters in practice and then evaluate the Jellybean protocol under different attack scenarios. The CSI samples used for parameter selection are collected in 90 second intervals, during which the LoS path of A - D channel in room A is interrupted by the occupant with artificial and daily activities. The approximate entropy of the fingerprint is calculated using the NIST randomness test suite [6]. Moreover, we obtained the p -value from the NIST tests which indicates if a sequence is sufficiently random to be used for security purposes. The p -value must exceed 0.01. For all the ApEn plots, we utilize empty markers to represent results with a p -value lower than 0.01, which indicates a failure in the NIST randomness test. Conversely, filled markers indicate a successful test.

Selecting W_m . The moving variance window W_m alleviates the high sensitivity of the CSI amplitude measurements. It needs to be long enough to smooth the rapid fluctuations, but should not eliminate the CSI randomness. Figure 6 presents the BMR and ApEn as a function of W_m for both artificial and natural daily activities. To simplify the analysis, W_m is converted from the number of CSI samples to seconds based on the sampling rate. We choose the smallest W_m value that results in a BMR of less than 0.2 and an ApEn with p -values exceeding 0.01. As a result, we set W_m to 0.1s for artificial activities and 0.25s for daily activities. This selection balances the functionality and security of the Jellybean protocol while ensuring a sufficiently random fingerprint is generated.

Selecting W_s . The averaging window W_s provides an additional level of smoothing to account for imperfect channel reciprocity and the sensitivity of the mmWave channel to small changes in geometry. It is also of great significance to avoid prolonging W_s that can result in a predictable fingerprint. In Figure 8, we show the BMR and ApEn as a function of W_s . We observe that the BMR monotonically decreases as W_s increases. However, compared to W_m , the Jellybean protocol is more sensitive to changes in W_s , and

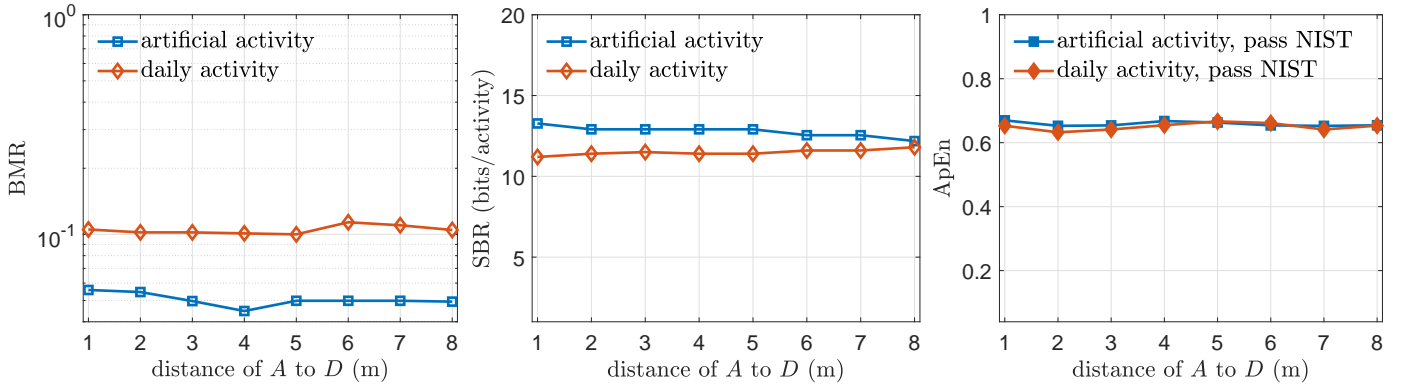


Figure 7: Performance evaluation of Jellybean with two types of activities in room B.

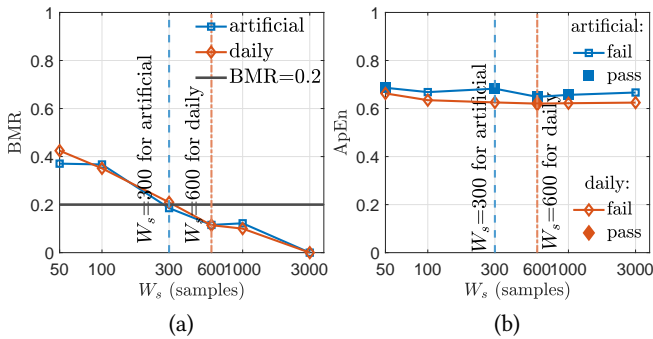


Figure 8: (a) BMR as a function of W_s , and (b) ApEn as a function of W_s .

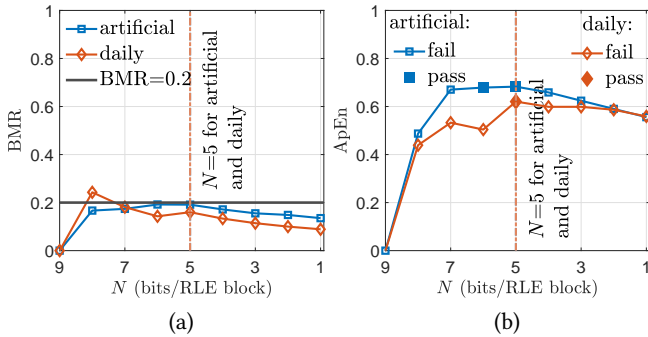


Figure 9: (a) BMR as a function of N , and (b) ApEn as a function of N .

the generated fingerprint can easily become predictable, failing the NIST randomness test for many W_s values. We choose the smallest W_s value that yields a BMR below 0.2 and an ApEn with a p -value greater than 0.01, indicating a usable fingerprint. Consequently, we let $W_s = 300$ and $W_s = 600$ for artificial and daily activities, respectively.

Selecting N . The number of LSBs maintained from each CSI block control the contribution of each event (activity or inactivity) to the final bit sequence used as fingerprint. The selection of N also impacts the entropy of the final bit sequence as a longer N could lead to more predictable sequences. Figure 9 shows how BMR and ApEn vary with N . As expected, a smaller N leads to a higher

BMR but also a higher ApEn. To best balance the functionality and security of the Jellybean protocol, we fix $N = 5$ for both artificial and daily activities.

Selecting the RS code. The final parameter to be selected is the RS code used in the key agreement phase. The code's error correcting capability must be high enough to allow for the observed BMR, but low enough so that k is not leaked to Mallory. Based on the previously selected parameters and the obtained BMR values, we considered an RS code that tolerated a 20% mismatch between the two fingerprints. This is inline with codes used in previous context-based methods.

4.4 Performance Evaluation of Jellybean

In this section, we evaluate the performance of Jellybean protocol using the parameters set above. To test the protocol robustness to environmental changes, we conducted additional experiments in room B. Room B has a larger space and a more complicated RF environment compared to room A. The layout of Room B is shown in Figure 5(c). We conducted additional experiments in room B, shown in Figure 5(c), to illustrate varying A - D 's distance impact on evaluation metrics BMR, SBR, and ApEn. We varied the distance between A and D from 1m to 8m. For each distance, we collected CSI samples for three minutes while performing artificial and natural daily activities. Figure 7 shows the BMR, SBR, and ApEn at different distances. We observe a sound trend of the three metrics, which indicates that the AF algorithm can develop activity-based fingerprints with a low BMR, an acceptable SBR, and NIST-approved ApEn.

4.5 Security Analysis for Jellybean

In this section, we analyze the security of our Jellybean protocol against different types of adversaries.

1) Eavesdropping Adversary: We first consider an eavesdropper M is positioned at the same distance from A as D . This positioning is intended to ensure a similar channel loss for A - M channel as for A - D channel, thereby enabling M to actively adjust its angle from the A - D channel to identify the best eavesdropping opportunities. Due to the hardware limitation, we only used four USRPs N200 to implement A , D , and M , as shown in Figure 10(a). We maintained the distance for A - D and A - M links as 4m and collected

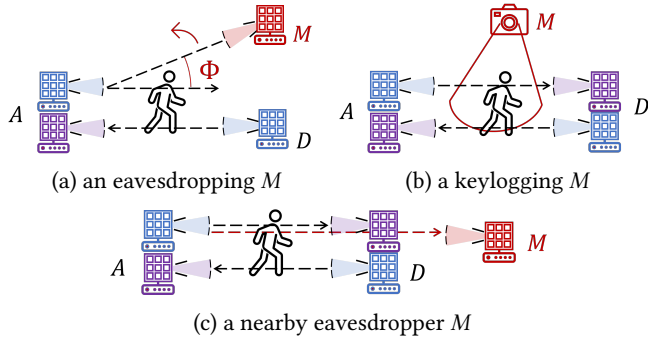
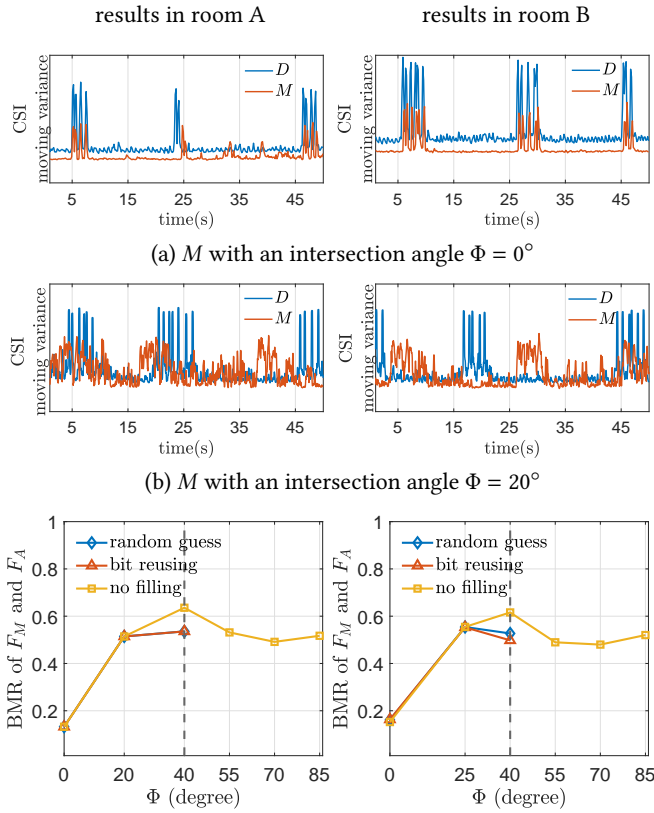


Figure 10: Experiment settings for evaluating Jellybean with different types of M .

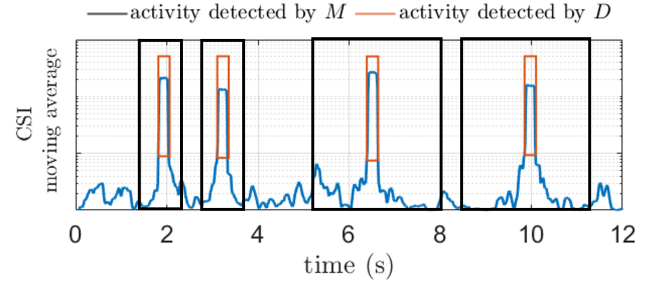


(c) BMR of F_A and F_M as a function of Φ , F_M after the dash line is generated with random guess due to the trivial CSI samples received at M .

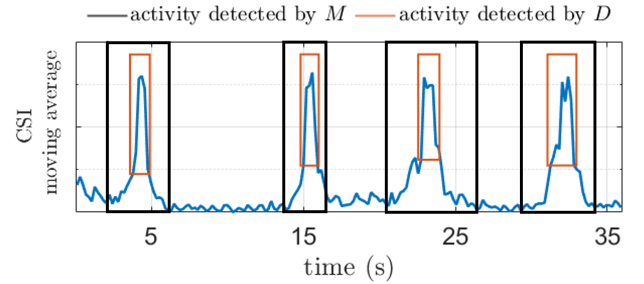
Figure 11: Evaluation of Jellybean for an eavesdropping M in room A (the left column) and room B (the right column).

2-minute CSI samples with different angles Φ between A - D and A - M channels. To ensure fairness, activities were conducted near hub A , allowing activities observations for both D and M .

Due to the directionality of the directional beam produced by the phased array beamformer, the probing signal emitted by A gets lost at M when Φ exceeds a certain value. To compensate the sample loss and compare the fingerprint of M with that of A , we fill in the corresponding missing bits in F_M to ensure that F_A and



(a) artificial activity



(b) daily activity

Figure 12: Security evaluation of the Jellybean for a keylogging M with two types of activities in experimental room A.

F_M have the same length. We employed three strategies for this purpose: 1) random guess that involves randomly filling in a bit to replace the missing one in F_M , 2) bit reusing that reuses a segment of previously extracted bits from F_M , and 3) no filling that leaves the missing bit blank. Figure 11(c) shows the BMR between F_A and F_M as a function of Φ for these three strategies. We observed a high BMR between F_A and F_M , except when $\Phi = 0^\circ$. Figures 11(a) and (b) further present the moving variance of the 45-second CSI samples collected by D and M , respectively, for $\Phi = 0^\circ$ and $\Phi = 20^\circ$. When $\Phi = 20^\circ$, there is a significant difference in observations between D and M , resulting in a failed key agreement process at M . However, when M perfectly aligns with the A - D link at $\Phi = 0^\circ$, she can successfully retrieve the agreed key between A and D based on her own observations, which exhibit a relatively low BMR of 0.2. Such a strong eavesdropper is referred to as a *nearby* eavesdropper and we introduce an upgraded protocol called Jellybean+ in Sec. 5 to thwart it. In summary, the basic Jellybean protocol is secure against a co-located eavesdropper outside the close proximity to A or D .

2) Keylogging Adversary: A keylogging adversary uses vision instead of RF devices for activity fingerprinting. M monitors all the activities taking place in the shared area between A and D with a camera, as shown in Figure 10(c). She determines the start and ending time for each activity by examining all the video recordings frame by frame and fingerprints the activity by filling bits 1s in the duration of each activity and 0s for the rest.

We let the keylogging adversary record the activities with a cell phone and we evaluate the performance of it by comparing the start and end time of the activities extracted by M and D . Figure 12 shows the activity detection results for D and M with one artificial and

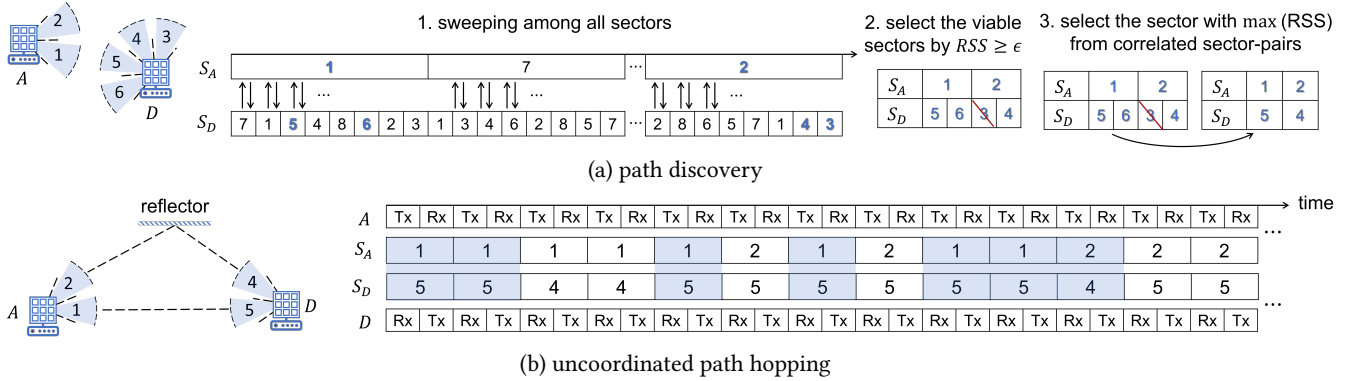


Figure 13: An example of the path discovery phase and path hopping phase in UPH. The numbers indicate the chosen sectors at each device. If A and D simultaneously switch to a usable sector pair (2-4 and 1-5 in the example), the probing round is successful and activities are measured.

daily activity, respectively. We can see that due to the denoising and smoothing process in the Jellybean protocol, D detects the duration of one artificial activity in a range of 0.08-0.1 seconds, whereas M records a longer duration spanning 1-3 seconds for the same activity. Similarly, for daily activities, M detects the activity with a significantly longer duration compared to D . This substantial discrepancy in activity fingerprinting between M and D makes it impossible for M to agree on the same key as established between A and D .

3) Beam-stealing Adversary. M deceives A and D by manipulating the beam alignment process. M forges sector sweep frames with high received signal strength (RSS), leading A and D to align their beams with M instead of each other [38]. This beam-stealing attack allows M to launch a MitM attack against the pairing protocol.

The basic Jellybean protocol is vulnerable to this attack due to the lack of authentication in the beam alignment process. With the amended Jellybean+ protocol introduced in Sec. 5, we remove the assumption of beam alignment and instead employ an uncoordinated path-hopping (UPH) mechanism. This approach takes advantage of multiple paths and utilizes the electronic antenna steering capabilities of mmWave technology to randomize the activity sensing area. By adopting Jellybean+, we not only defend against the strong nearby eavesdropper, but we also mitigate the threat posed by an active beam-stealing adversary.

5 UNCOORDINATED PATH HOPPING

Based on the security analysis, the activity fingerprinting process is vulnerable to two attacks. First, a passive adversary that is aligned with the path observed by A and D will extract a similar fingerprint to F_A and F_D (with a BMR below 0.2 as seen in Figure 11(c)), thus also being able to obtain k from the commitment value δ_A . Second, an active adversary launching a beam-stealing attack can become a MitM between A and D . In this scenario, M can independently establish keys with A and D using the activities in the $A-M$ and the $M-D$ paths, respectively.

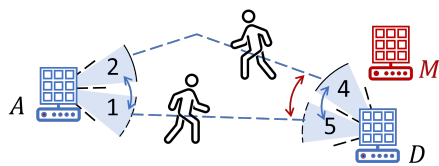
To prevent these attacks, we propose the *Jellybean+* protocol that exploits the potential availability of multiple communication paths between A and D (e.g., LoS path and one reflection path). The main idea is to “hop” (steer) the antennas between paths and

merge activities from each path (direction) into the same fingerprint. Without knowing which path to monitor at any given time, Mallory cannot extract the same fingerprint, even if she can observe all paths. Likewise, in a beam-stealing attack scenario, the activities toward the direction of Mallory contribute to the fingerprint only partially, since activities on other paths are also present. Evidently, path hopping is similar to frequency hopping but applied in the space domain as opposed to the frequency domain.

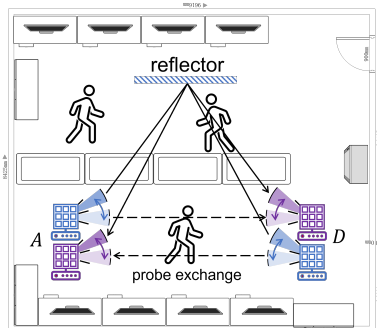
There are two main challenges for applying path hopping in our context, due to the lack of initial trust. First, how do A and D discover viable communication paths (paths where probe decoding is possible) and second, how do A and D securely share a common path hopping sequence. We address both challenges by developing an *uncoordinated path-hopping mechanism* (UPH), where A and D hop independently between the available paths. The UPH mechanism has two phases; the path discovery phase and the path hopping phase.

1. Path discovery. To discover the available paths between A and D , we propose a new beam alignment process that keeps track all transmitter-receiver antenna sector combinations that yield an RSS that exceeds the receiver’s sensitivity by a margin ϵ . The path discovery process is demonstrated in Figure 13(a). Both A and D sweep the plane but with different periods. A sweeps slowly whereas D sweeps fast. The protocol proceeds in rounds. During a round, A fixes its antenna at one sector whereas D sweeps through all sectors in random order. Consider A pointing to S_A whereas D is pointing to S_D . Device D sends a probe (sector sweep frame) to A . If the probe is correctly decoded and the RSS exceeds the receiver sensitivity by the margin ϵ , A replies with each own probe from sector S_A . If A ’s probe is also decodable, D records sector S_D as viable and responds to A with an ACK. Upon reception of the ACK, A also records S_A as viable. This process is repeated for every sector of D , while A remains on the same sector. If multiple sectors of D can be received by A , D chooses the strongest one (highest RSS). In the next round, A randomly switches to another sector and the probing process is repeated.

At the end of the path discovery process, each party learns the set of viable sectors that can achieve communication with the other party. Note that each party only knows its own viable sectors. In the example of Figure 13(a), we show several rounds of path discovery.



(a) Passive adversary close to D .



(b) Setup for Jellybean+

Figure 14: (a) passive threat model and (b) experiment setup.

In round 1, A steers to sector $S_A = 1$ while D sweeps through all eight sectors. Successful communication takes place in sector pairs 1 – 5 and 1 – 6. A records sector 1 as a viable sector and D records sectors 5 and 6 as viable sectors. Because the RSS on sector 5 is higher, only sector 5 is recorded. The process is repeated on future rounds. At the completion of 8 rounds, two paths yield viable directions, namely 1-5 (LoS) and 2-4 (reflection).

2. Uncoordinated path hopping. In the next phase, A and D hop through their viable sectors in an uncoordinated fashion. The dwell time on each sector is sufficient to exchange several probes. If the probes are successfully exchanged, both devices record the CSI as part of the set used to generate each fingerprint. Otherwise, the CSI samples are discarded. In Figure 13(b) we show A and D hopping in an uncoordinated fashion between their viable sectors discovered in Figure 13(a). Only the blue pairs result in successful probe exchanges that are used for fingerprint generation.

5.1 Security Analysis of Jellybean+

The security of Jellybean+ hinges on the unpredictability of the path that is sampled at any given time. Because the antennas are independently steered, Mallory does not know which paths are being sampled, unless she can capture all probes at all times.

Resistance to passive adversaries. We first consider the case where M is positioned close to one of the devices, say D , such that it can observe similar viable paths as D . This model is shown in Figure 14(a). This adversary was shown to be capable of extracting a similar fingerprint as D if only the LoS path was used. To evaluate Jellybean+, we assume the best case for M where she knows all viable paths identified during the path discovery process. Referring to the example of Figure 13(a), this would correspond to knowing that paths 1-5 and 2-4 were discovered. This could be inferred by either knowing the device topology or intercepting probe messages. To measure the same fingerprint F_D , Mallory must hop between the viable paths in an uncoordinated fashion, similar to A and D . The probability of extracting the same fingerprint equals the probability

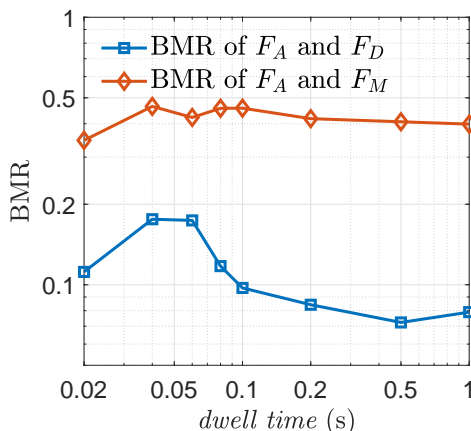


Figure 15: Security evaluation of the Jellybean+ when M is co-located with D , where BMR between $A - D$ and $A - M$ as a function of the path dwell time.

of following the same path sequence as D for the fraction of hops that correspond to viable paths (blue-shaded slots in Figure 13 (b)). This probability is expressed in the following proposition.

PROPOSITION 5.1. *Let A and D hop between P viable paths using uncoordinated sequences that match at Q hops. The probability that M extracts the same fingerprint as D is given by*

$$Pr[F_M = F_D] = \left(\frac{1}{P}\right)^Q.$$

PROOF. To measure the same fingerprint F_D , M must steer her antenna to the same sector as D on all of the Q hops where viable paths are observed. Each hop in the sequence is randomly selected out of P paths with probability $1/P$. Matching a single hop occurs with the same probability of selecting the specific path out of P paths, which is equivalent to a Bernoulli trial with success probability $1/P$. Each hop in the hopping sequence is selected independently, making the probability of matching X out of Q hops follow the binomial distribution $B(Q, 1/P)$. Because we want all Q hops to match it follows that $Pr[F_M = F_D] = P(Q) = (1/P)^Q$. \square

Remark 1: Proposition 1 holds even if Mallory is equipped with P antennas that can sample physical activity on all P paths simultaneously. This is because Mallory is not aware of where D steers its antenna at every hop and therefore she has to guess which of the P paths she should include in the CSI sample set. A correct guess occurs with probability $1/P$ independently at each viable hop, yielding Proposition 1.

Remark 2: When relaxing the fingerprint matching condition to only K out of Q paths, the probability of inferring a similar fingerprint to F_D is given by the binomial distribution $B(Q, 1/P)$, with K out of Q successes.

Note that we cannot analytically derive the probability of inferring the key k (equivalently the BMR between F_D and F_M) because it depends on the start time and duration of the observed activities on each path. We experimentally evaluated the BMR of the adversary under the UPH protocol, using the setup shown in Figure 14(b). During the path discovery phase, A and D discovered two paths,

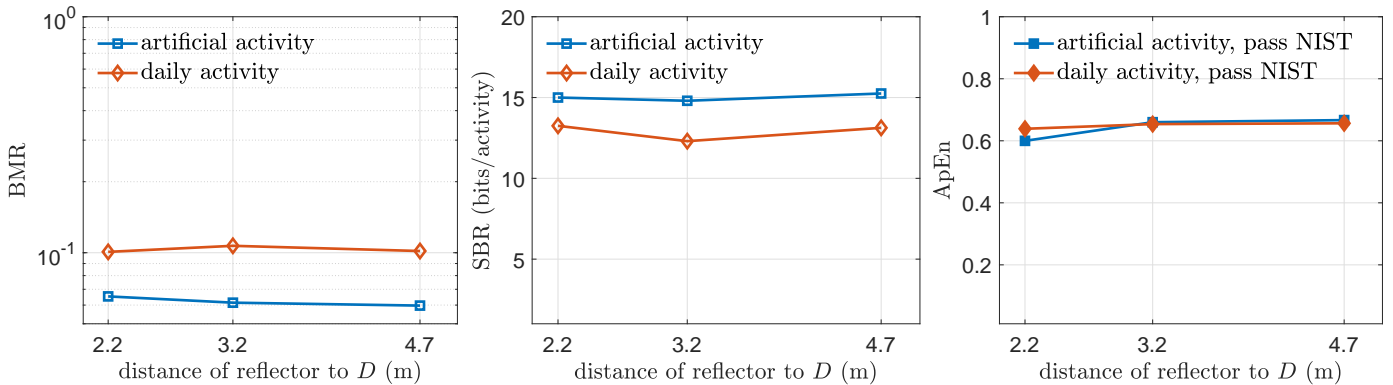


Figure 16: Performance evaluation of the Jellybean+ with two types of activities in experimental room B, where the evaluation metrics BMR, SBR, and ApEn are captured in a function of the distances of D to the reflector on the $A - D$ NLoS path.

one through the LoS and one through the reflector. We collected CSI samples on each of those paths for 25 minutes independently. We generated hopping sequences at A , D , and M independently, and varied the *dwelt time* on each path from 0.02 seconds to 1 second. We then followed the uncoordinated path hopping mechanism between A and D according to the generated hopping sequences and recorded the BMR. The adversary recorded CSI samples, only when it could hear probes from A .

Figure 15 shows the BMR as a function of the dwell time on each path. We observe that the BMR between F_A and F_D remain unaffected by the introduction of UPH. On the other hand, the BMR between F_A and F_M is approximately 0.5 which equals the probability of guessing the correct path at every hop. The success probability is also equal to the probability of randomly guessing k , indicating that the adversary gains no advantage by attempting to observe activities from nearby when path diversity is exploited.

Note that the BMR remains relatively constant for all dwell times. This is because M hopped paths with the same period as D . Hopping between paths at a shorter period is not beneficial to the adversary because (a) it will miss receiving probes that are essential for determining the activity start time and duration and (b) it still has to guess which paths contribute to the fingerprints (Remark 1).

Resistance to active adversaries. We now describe how Jellybean+ can prevent active attacks. An active attack relies on beam-stealing to place Mallory in control of the probe exchange between A and D , so that M can independently establish keys with A and D , using parallel pairing sessions (MitM). The beam-stealing attack is possible, because the beam alignment protocol results in the use of a single path (the best path) between two communicating devices. With UPH, multiple paths are used to extract activity fingerprints. Even if the adversary controls one or a subset of those paths, she still needs to guess when A and D sample the remaining attack-free paths. Moreover, M cannot sample other paths she does not control unless she simultaneously deploys passive eavesdroppers that are aligned to those paths. In this case, the results obtained for passive adversaries (Proposition 1 and Figure 15) hold for the active adversary. As long as there are more than one paths not controlled by M , the probability of matching fingerprints decays exponentially with the hopping sequence length.

5.2 Performance Evaluation of Jellybean+

Time analysis. One concern with UPH is that the uncoordinated hopping will introduce a long delay until devices can measure sufficiently long fingerprints. To alleviate this concern, we analyze the time for fingerprint generation. The path discovery phase is deterministic and requires the operation of N full sweeps from D where N is the number of available sector (N^2 hops in total). In each hop, A and D exchange two probes (sector sweep frame) and a sweep ACK. Using parameters from the IEEE 802.11ad specification [2], each probe is 26 bytes long whereas a sweep ACK is 28 bytes long. Moreover, the time interval between two probes for beam switching, called the short beamforming interframe spacing (SB-IFS) is $T_s = 1\mu s$. Assuming a 160Mbps transmission rate, the time consumed during path discovery is 5.12ms.

The delay for fingerprint extraction during the UPH phase is similar to that of Jellybean if the dwell time is selected to be low (e.g., less than 0.1sec). This is because path hopping is much faster than the activity timescale, so that all activities occurring on any of the viable paths will be intermittently sampled.

Performance on the reflection path. Since Jellybean+ uses a reflection path, we explored the the BMR, SBR, and ApEn on that path. We varied the distance between D and the reflector as depicted in room B of Figure 5(c). The experiments were executed for 3 minutes under each distance with artificial and natural daily activities. Figure 16 shows the BMR, SBR, and APEn for the two types of activities. We observe that the BMR, SBR, and ApEn have similar values to those obtained in the LoS path for each activity type, despite the lower RSS on the reflected path. The use of CSI variance is a strong indicator of activity and inactivity. In fact, the reflected path is easier to disrupt due to its higher attenuation.

6 RELATED WORK

Context-based Device Pairing. Our proposed protocol belongs to the general category of context-based device pairing protocols. Such protocols aim to establish a shared secret key between two wireless devices by sensing common contexts that are dynamic and random, without relying on any pre-shared secrets such as passcodes. They provide notable advantages such as reduced user efforts, perpetual key renewal, and a high level of security against

remote adversaries. Commonly explored physical modalities in context-based pairing include ambient light [25], sound [25, 32, 51], human operation [17, 56]. However, all the above methods require that all the devices possess the same sensing modality, which can be impractical for real-world applications such as IoT. Recently, several works addressed this limitation by using multi-modal sensing [8, 10] for common activity detection, which is applicable to devices with heterogeneous sensing capabilities. However, the types of activities that can be simultaneously sensed by different sensors are limited. Most importantly, all those methods are only secure against a passive adversary which is located outside of the physical context (e.g., a room where the legitimate devices are located).

On the other hand, other works such as [11, 19, 21, 23, 24, 28, 55] used the (in-band) radio interface to sense ambient RF signals do not require devices to possess a common sensor other than the same RF interface which is widely existed. They have leveraged the correlation of measured ambient RF signals (e.g., RSS) to securely pair two or more devices that are co-located or in proximity [23, 33, 50]. However, RF signals decorrelate fast when the distance increases (usually not correlated beyond half wavelength), which requires very small proximity ranges (e.g., 12.5 cm at 2.4GHz, and millimeter range for mmWave frequencies) that are impractical for many applications. In [53], large-scale fading of RF signals is leveraged for verification of continuous proximity, which has a larger correlation distance, but it is applicable to outdoor mobile settings and not in the mmWave band. In contrast, our protocol does not limit the distance between the legitimate devices as long as they are within each other's communication range. Also, it is secure against an adversary in the same environment (even in close proximity to legitimate devices).

Security of mmWave Communications. Early works on the security of mmWave focused on ensuring message confidentiality against passive adversaries. mmWave is generally considered to be more secure against eavesdropping due to its highly directional transmissions. Indeed, this is the case when the adversary is located outside of the beam of a mmWave link. Yet, Steinmetzer et al. [37] demonstrated that eavesdropping is still possible if the adversary can place a reflector within the beam to deflect the signal. There are also works that leverage channel reciprocity to extract secret keys from a mmWave link [13, 14, 16], however, it is challenging since the entropy is low under static channel environments, while channel reciprocity may not hold for dynamic channels due to the high sensitivity of mmWave signals.

On the other hand, several works studied the security of mmWave communication against active attacks such as impersonation or MitM. Balakrishnan et al. [4] studied device fingerprinting based on variations in their beam patterns, in order to prevent impersonation attacks. Wang et al. [44, 45] adopted a similar approach by using machine learning algorithms to extract unique beam patterns for each device, enabling the receiver to distinguish devices and detect spoofing attacks. However, these methods require training, which incur extra overhead and complexity, and it is impractical to obtain secure training data when new devices join the network. Steinmetzer et al. [36] first demonstrated the beam-stealing attack against the 802.11ad protocol for mmWave communications, and proposed an authenticated beam sweep protocol that integrates crypto machinery to protect it against beam-stealing. However, in

the device pairing problem, there is no prior trust which makes such an approach inapplicable.

Wireless Sensing for Human Activity Detection and Recognition (HAR). Our work is also related to wireless sensing, especially passive sensing where the wireless transceivers are deployed in the environment rather than on the objects of interest. Existing works in this domain typically extract features from the CSI of the received wireless signals to detect or recognize human activity, based on the fact that different activities will incur different disturbances to the CSI. For example, in sub-6GHz bands, WiFi signals have been widely used for activity sensing [9, 41, 43, 47, 49]. Meanwhile, due to the high bandwidth and sensing resolution of mmWave signals, mmWave sensing has attracted increasing attention in recent years [12, 18, 20, 34, 40, 42, 46, 48].

Our work differs from HAR, since our activity fingerprinting method only aims at detecting the presence or absence (timing) of an activity, rather than classifying the type of activity. In contrast, human activity recognition typically relies on machine learning methods which require a large amount of training data. It is impractical to collect sufficient and secure training data in device pairing scenarios (where the devices meet for the first time without prior trust). In our protocol, we only require that the devices can observe common events' timing, thus training is not needed.

7 CONCLUSION

We proposed Jellybean, a novel secret-free pairing protocol for devices operating in the mmWave band. Our basic idea is to leverage in-band mmWave communications to detect (human) activities present in the physical environment as the common context. Jellybean extracts activity timing information via CSI measurements, which is used as a source of shared entropy for key agreement. We further enhance the security of the basic scheme with an uncoordinated path hopping mechanism, which achieves activity detection using directional beams under the absence of prior trust. The key novelty of Jellybean originates from exploiting the unique properties of mmWave signals to defend against both co-located passive adversaries as well as active adversaries. We evaluated Jellybean experimentally in two indoor environments, and showed that it can securely pair devices in the same room while thwarting adversaries located in the same space.

REFERENCES

- [1] [n. d.]. <https://www.tmytek.com/solutions/mmW-SDR>
- [2] 2012. IEEE Standard for Information technology—Telecommunications and information exchange between systems—Local and metropolitan area networks—Specific requirements—Part 11: Wireless LAN Medium Access Control (MAC) and Physical Layer (PHY) Specifications Amendment 3: Enhancements for Very High Throughput in the 60 GHz Band.
- [3] Mustafa Riza Akdeniz, Yuanpeng Liu, Mathew K Samimi, Shu Sun, Sundeeep Rangan, Theodore S Rappaport, and Elza Erkip. 2014. Millimeter wave channel modeling and cellular capacity evaluation. *IEEE journal on selected areas in communications* 32, 6 (2014), 1164–1179.
- [4] Sarankumar Balakrishnan, Shreya Gupta, Arupjyoti Bhuyan, Pu Wang, Dimitrios Koutsonikolas, and Zhi Sun. 2019. Physical layer identification based on spatial-temporal beam features for millimeter-wave wireless networks. *IEEE Transactions on Information Forensics and Security* 15 (2019), 1831–1845.
- [5] Sarankumar Balakrishnan, Pu Wang, Arupjyoti Bhuyan, and Zhi Sun. 2019. Modeling and analysis of eavesdropping attack in 802.11 ad mmWave wireless networks. *IEEE Access* 7 (2019), 70355–70370.
- [6] Lawrence E Bassham III, Andrew L Rukhin, Juan Soto, James R Nechvatal, Miles E Smid, Elaine B Barker, Stefan D Leigh, Mark Levenson, Mark Vangel, David L

- Banks, et al. 2010. *Sp 800-22 rev. 1a. a statistical test suite for random and pseudo-random number generators for cryptographic applications*. National Institute of Standards & Technology.
- [7] Simon Eberz, Martin Strohmeier, Matthias Wilhelm, and Ivan Martinovic. 2012. A practical man-in-the-middle attack on signal-based key generation protocols. In *Computer Security—ESORICS 2012: 17th European Symposium on Research in Computer Security, Pisa, Italy, September 10-12, 2012. Proceedings 17*. Springer, 235–252.
- [8] Habiba Farrukh, Muslum Ozgur Ozmen, Faik Kerem Ors, and Z Berkay Celik. 2022. One Key to Rule Them All: Secure Group Pairing for Heterogeneous IoT Devices. In *2023 IEEE Symposium on Security and Privacy (SP)*. IEEE Computer Society, 1693–1709.
- [9] Ruiyang Gao, Mi Zhang, Jie Zhang, Yang Li, Enze Yi, Dan Wu, Leye Wang, and Daqing Zhang. 2021. Towards position-independent sensing for gesture recognition with Wi-Fi. *Proceedings of the ACM on Interactive, Mobile, Wearable and Ubiquitous Technologies* 5, 2 (2021), 1–28.
- [10] Jun Han, Albert Jin Chung, Manal Kumar Sinha, Madhumitha Harishankar, Shijia Pan, Hae Young Noh, Pei Zhang, and Patrick Tague. 2018. Do you feel what I hear? Enabling autonomous IoT device pairing using different sensor types. In *2018 IEEE Symposium on Security and Privacy (SP)*. IEEE, 836–852.
- [11] Suman Jana, Sriram Nandha Premnath, Mike Clark, Sneha K Kaseria, Neal Patwari, and Srikanth V Krishnamurthy. 2009. On the effectiveness of secret key extraction from wireless signal strength in real environments. In *Proceedings of the 15th annual international conference on Mobile computing and networking*. 321–332.
- [12] Wenjun Jiang, Chenglin Miao, Fenglong Ma, Shuochao Yao, Yaqing Wang, Ye Yuan, Hongfei Xue, Chen Song, Xin Ma, Dimitrios Koutsonikolas, et al. 2018. Towards environment independent device free human activity recognition. In *Proceedings of the 24th annual international conference on mobile computing and networking*. 289–304.
- [13] Long Jiao, Jie Tang, and Kai Zeng. 2018. Physical layer key generation using virtual AoA and AoD of mmWave massive MIMO channel. In *2018 IEEE Conference on Communications and Network Security (CNS)*. IEEE, 1–9.
- [14] Long Jiao, Ning Wang, Pu Wang, Amir Alipour-Fanid, Jie Tang, and Kai Zeng. 2019. Physical layer key generation in 5G wireless networks. *IEEE Wireless Communications* 26, 5 (2019), 48–54.
- [15] Ari Juels and Martin Wattenberg. 1999. A fuzzy commitment scheme. In *Proceedings of the 6th ACM conference on Computer and communications security*. 28–36.
- [16] Guyue Li, Chen Sun, Junqing Zhang, Eduard Jorswieck, Bin Xiao, and Aiqun Hu. 2019. Physical layer key generation in 5G and beyond wireless communications: Challenges and opportunities. *Entropy* 21, 5 (2019), 497.
- [17] Xiaopeng Li, Qiang Zeng, Lannan Luo, and Tongbo Luo. 2020. T2pair: Secure and usable pairing for heterogeneous iot devices. In *Proceedings of the 2020 acm sigsac conference on computer and communications security*. 309–323.
- [18] Jaime Lien, Nicholas Gillian, M Emre Karagozler, Patrick Amihoud, Carsten Schwesig, Erik Olson, Hakim Raja, and Ivan Poupyrev. 2016. Soli: Ubiquitous gesture sensing with millimeter wave radar. *ACM Transactions on Graphics (TOG)* 35, 4 (2016), 1–19.
- [19] Hongbo Liu, Yang Wang, Jie Yang, and Yingying Chen. 2013. Fast and practical secret key extraction by exploiting channel response. In *2013 Proceedings IEEE INFOCOM*. IEEE, 3048–3056.
- [20] Haipeng Liu, Yuheng Wang, Anfu Zhou, Hanyue He, Wei Wang, Kunpeng Wang, Peilin Pan, Yixuan Lu, Liang Liu, and Huadong Ma. 2020. Real-time arm gesture recognition in smart home scenarios via millimeter wave sensing. *Proceedings of the ACM on interactive, mobile, wearable and ubiquitous technologies* 4, 4 (2020), 1–28.
- [21] Hongbo Liu, Jie Yang, Yan Wang, and Yingying Chen. 2012. Collaborative secret key extraction leveraging received signal strength in mobile wireless networks. In *2012 Proceedings IEEE Infocom*. IEEE, 927–935.
- [22] Yanpei Liu, Stark C Draper, and Akbar M Sayeed. 2012. Exploiting channel diversity in secret key generation from multipath fading randomness. *IEEE Transactions on information forensics and security* 7, 5 (2012), 1484–1497.
- [23] Suhas Mathur, Robert Miller, Alexander Varshavsky, Wade Trappe, and Narayan Mandayam. 2011. Proximate: proximity-based secure pairing using ambient wireless signals. In *Proc. of the 9th MobiSys*.
- [24] Suhas Mathur, Wade Trappe, Narayan Mandayam, Chunxuan Ye, and Alex Reznik. 2008. Radio-telepathy: extracting a secret key from an unauthenticated wireless channel. In *Proceedings of the 14th ACM international conference on Mobile computing and networking*. 128–139.
- [25] Markus Miettinen, Nadarajah Asokan, Thien Duc Nguyen, Ahmad-Reza Sadeghi, and Majid Sobhani. 2014. Context-based zero-interaction pairing and key evolution for advanced personal devices. In *Proceedings of the 2014 ACM SIGSAC conference on computer and communications security*. 880–891.
- [26] Yanjun Pan, Ziqi Xu, Ming Li, and Loukas Lazos. 2021. Man-in-the-middle attack resistant secret key generation via channel randomization. In *Proceedings of the Twenty-second International Symposium on Theory, Algorithmic Foundations, and Protocol Design for Mobile Networks and Mobile Computing*. 231–240.
- [27] Steven M Pincus. 1991. Approximate entropy as a measure of system complexity. *PNAS* 88, 6 (1991), 2297–2301.
- [28] Sriram Nandha Premnath, Suman Jana, Jessica Croft, Prarthana Lakshmane Gowda, Mike Clark, Sneha Kumar Kaseria, Neal Patwari, and Srikanth V Krishnamurthy. 2012. Secret key extraction from wireless signal strength in real environments. *IEEE Transactions on mobile Computing* 12, 5 (2012), 917–930.
- [29] Theodore S Rappaport. 2010. *Wireless communications: Principles and practice, 2/E*. Pearson Education India.
- [30] Theodore S. Rappaport, Yunchou Xing, George R. MacCartney, Andreas F. Molisch, Evangelos Mellios, and Jianhua Zhang. 2017. Overview of Millimeter Wave Communications for Fifth-Generation (5G) Wireless Networks—With a Focus on Propagation Models. *IEEE Transactions on Antennas and Propagation* 65, 12 (2017), 6213–6230. <https://doi.org/10.1109/TAP.2017.2734243>
- [31] P. Rousseeuw and C. Croux. 1993. Alternatives to the median absolute deviation. *JASA* 88, 424 (1993), 1273–1283.
- [32] Dominik Schürmann and Stephan Sigg. 2011. Secure communication based on ambient audio. *IEEE TMC* 12, 2 (2011), 358–370.
- [33] Lu Shi, Ming Li, Shucheng Yu, and Jiawei Yuan. 2012. BANA: Body area network authentication exploiting channel characteristics. In *Proceedings of the fifth ACM conference on Security and Privacy in Wireless and Mobile Networks*. 27–38.
- [34] Akash Deep Singh, Sandeep Singh Sandha, Luis Garcia, and Mani Srivastava. 2019. Radhar: Human activity recognition from point clouds generated through a millimeter-wave radar. In *Proceedings of the 3rd ACM Workshop on Millimeter-wave Networks and Sensing Systems*. 51–56.
- [35] William Stallings, Lawrie Brown, Michael D Bauer, and Michael Howard. 2012. *Computer security: principles and practice, Vol. 3*. Pearson Upper Saddle River.
- [36] D. Steinmetzer, S. Ahmad, N. Anagnostopoulos, M. Hollick, and S. Katzenbeisser. 2018. Authenticating the sector sweep to protect against beam-stealing attacks in IEEE 802.11 ad networks. In *Proc. of the 2nd ACM Workshop on mmNets*.
- [37] Daniel Steinmetzer, Joe Chen, Jiska Classen, Edward Knightly, and Matthias Hollick. 2015. Eavesdropping with periscopes: Experimental security analysis of highly directional millimeter waves. In *2015 IEEE Conference on Communications and Network Security (CNS)*. IEEE, 335–343.
- [38] Daniel Steinmetzer, Yimin Yuan, and Matthias Hollick. 2018. Beam-stealing: Intercepting the sector sweep to launch man-in-the-middle attacks on wireless IEEE 802.11 ad networks. In *Proc. of the 11th ACM WiSec*. 12–22.
- [39] Mario Strasser, Christina Popper, Srdjan Capkun, and Mario Galaj. 2008. Jamming-resistant key establishment using uncoordinated frequency hopping. In *2008 IEEE Symposium on Security and Privacy (sp 2008)*. IEEE, 64–78.
- [40] Yangfan Sun, Renlong Hang, Zhu Li, Mouqing Jin, and Kelvin Xu. 2019. Privacy-preserving fall detection with deep learning on mmWave radar signal. In *2019 IEEE Visual Communications and Image Processing (VCIP)*. IEEE, 1–4.
- [41] Sheng Tan and Jie Yang. 2016. WiFinger: Leveraging commodity WiFi for fine-grained finger gesture recognition. In *Proceedings of the 17th ACM international symposium on mobile ad hoc networking and computing*. 201–210.
- [42] Baptist Vandersmissen, Nicolas Knudde, Azarakhsh Jalalvand, Ivo Couckuyt, Tom Dhaene, and Wesley De Neve. 2020. Indoor human activity recognition using high-dimensional sensors and deep neural networks. *Neural Computing and Applications* 32 (2020), 12295–12309.
- [43] Raghav H Venkatnarayan, Griffin Page, and Muhammad Shahzad. 2018. Multi-user gesture recognition using WiFi. In *Proceedings of the 16th Annual International Conference on Mobile Systems, Applications, and Services*. 401–413.
- [44] Ning Wang, Long Jiao, Pu Wang, Weiwei Li, and Kai Zeng. 2020. Machine learning-based spoofing attack detection in mmWave 60GHz IEEE 802.11 ad networks. In *IEEE INFOCOM 2020-IEEE Conference on Computer Communications*. IEEE, 2579–2588.
- [45] Ning Wang, Long Jiao, Pu Wang, Weiwei Li, and Kai Zeng. 2021. Exploiting Beam Features for Spoofing Attack Detection in mmWave 60-GHz IEEE 802.11 ad Networks. *IEEE Transactions on Wireless Communications* 20, 5 (2021), 3321–3335.
- [46] Saiwen Wang, Jie Song, Jaime Lien, Ivan Poupyrev, and Otmár Hilliges. 2016. Interacting with soli: Exploring fine-grained dynamic gesture recognition in the radio-frequency spectrum. In *Proceedings of the 29th Annual Symposium on User Interface Software and Technology*. 851–860.
- [47] Wei Wang, Alex X Liu, Muhammad Shahzad, Kang Ling, and Sanglu Lu. 2017. Device-free human activity recognition using commercial WiFi devices. *IEEE Journal on Selected Areas in Communications* 35, 5 (2017), 1118–1131.
- [48] Yuheng Wang, Haipeng Liu, Kening Cui, Anfu Zhou, Wensheng Li, and Huadong Ma. 2021. m-activity: Accurate and real-time human activity recognition via millimeter wave radar. In *ICASSP 2021-2021 IEEE International Conference on Acoustics, Speech and Signal Processing (ICASSP)*. IEEE, 8298–8302.
- [49] Yan Wang, Jian Liu, Yingying Chen, Marco Gruteser, Jie Yang, and Hongbo Liu. 2014. E-eyes: device-free location-oriented activity identification using fine-grained wifi signatures. In *Proceedings of the 20th annual international conference on Mobile computing and networking*. 617–628.
- [50] Yongpeng Wu, Ashish Khisti, Chengshan Xiao, Giuseppe Caire, Kai-Kit Wong, and Qiqi Gao. 2018. A survey of physical layer security techniques for 5G wireless networks and challenges ahead. *IEEE Journal on Selected Areas in Communications* 36, 4 (2018), 679–695.

- [51] Weitao Xu, Zhenjiang Li, Wanli Xue, Xiaotong Yu, Bo Wei, Jia Wang, Chengwen Luo, Wei Li, and Albert Y Zomaya. 2021. Inaudiblekey: Generic inaudible acoustic signal based key agreement protocol for mobile devices. In *Proc. of the 20th IPSN*.
- [52] Ziqi Xu, Jingcheng Li, Yanjun Pan, Loukas Lazos, Ming Li, and Nirnimesh Ghose. 2021. PoF: Proof-of-Following for Vehicle Platoons. *arXiv preprint arXiv:2107.09863* (2021).
- [53] Ziqi Xu, Jingcheng Li, Yanjun Pan, Loukas Lazos, Ming Li, and Nirnimesh Ghose. 2022. PoF: Proof-of-Following for Vehicle Platoons. In *Proceedings 2022 Network and Distributed System Security Symposium*.
- [54] Hongli Yu, Bin Yang, Jinjun Liu, and Gwo-Jong Yu. 2018. Passive human trajectory tracking study in indoor environment with CSI. In *IEEE NaNA*.
- [55] Kai Zeng, Daniel Wu, An Chan, and Prasant Mohapatra. 2010. Exploiting multiple-antenna diversity for shared secret key generation in wireless networks. In *2010 Proceedings IEEE INFOCOM*. IEEE, 1–9.
- [56] Tengxiang Zhang, Xin Yi, Ruolin Wang, Yuntao Wang, Chun Yu, Yiqin Lu, and Yuanchun Shi. 2018. Tap-to-pair: associating wireless devices with synchronous tapping. *Proceedings of the ACM on Interactive, Mobile, Wearable and Ubiquitous Technologies* 2, 4 (2018), 1–21.
- [57] Z. Zhang, J. Ryu, S. Subramanian, and A. Sampath. 2015. Coverage and channel characteristics of millimeter wave band using ray tracing. In *IEEE ICC*.
- [58] Y. Zhu, Z. Xiao, Y. Chen, Z. Li, M. Liu, B. Zhao, and H. Zheng. 2020. Et tu Alexa? When commodity WiFi devices turn into adversarial motion sensors. NDSS.